Available online at www.sciencedirect.com
ScienceDirect
Journal of Solid State Chemistry 179 (2006) 3556–3561
JOURNAL OF SOLID STATE CHEMISTRY
www.elsevier.com/locate/jssc

Compression mechanisms of symmetric and Jahn–Teller distorted octahedra in double perovskites: A_2CuWO_6 (A = Sr, Ba), Sr_2CoMoO_6, and La_2LiRuO_6

Michael W. Lufaso[a], William R. Gemmill[a], Samuel J. Mugavero III[a], Yongjae Lee[b], Thomas Vogt[a], Hans-Conrad zur Loye[a,*]

[a]*Department of Chemistry and Biochemistry, University of South Carolina, 631 Sumter Street, Columbia, SC 29208, USA*
[b]*Department of Earth System Sciences, Yonsei University, Seoul 120749, Republic of Korea*

Received 27 April 2006; received in revised form 21 June 2006; accepted 13 July 2006
Available online 16 July 2006

Abstract

Synchrotron X-ray powder diffraction was used to study the high pressure dependence of the lattice parameter and structural evolution of the monoclinic La_2LiRuO_6 and tetragonal Sr_2CoMoO_6, Sr_2CuWO_6, and Ba_2CuWO_6 double perovskite phases. The c lattice parameters of Sr_2CuWO_6 and Ba_2CuWO_6 decreased more rapidly than the a lattice parameters and Ba_2CuWO_6 exhibited a more anisotropic compression compared to Sr_2CuWO_6. Based on lower pressure refinements of Ba_2CuWO_6, the anisotropic compression is proposed to be due to the preferential compression of the Cu–O bonds containing cooperative Jahn–Teller distortions aligned parallel to the c-axis, which is in contrast to Sr_2CoMoO_6, where the change in the octahedral tilting and symmetric bond compression is the prevailing compression mechanism. The bulk moduli were obtained from a fit of the volume–pressure data using the second-order Murnaghan equation of state.

Keywords: High-pressure; Diamond anvil cell; Jahn–Teller; Bulk modulus; Equation of state; Octahedral tilting

1. Introduction

The structural and physical properties of perovskite compounds have been an active area of research because of the diverse physical properties and structural chemistry exhibited by this family of oxides [1]. The addition of a second B-cation, as in $AB_{0.5}B'_{0.5}O_3$, allows for the possibility of cation ordering in ABO_3 perovskites, particularly when there is a large difference in the oxidation state or size of B and B' [2]. The cuprate ordered double perovskites Ba_2CuWO_6 and Sr_2CuWO_6 have been investigated for their interesting structural and magnetic properties [3–8]. Both compounds contain Cu^{2+} octahedra prone to undergo a Jahn–Teller distortion [9,10]. Orbital ordering and alignment of the long Cu–O bonds occurs parallel to the c-axis along the fourfold axis. The interaction between orbital ordering and octahedral tilting of Cu^{2+} containing perovskites is different from Mn^{3+} containing compounds, where the long Mn–O bonds alternate in a plane [11]. Thereby, we are able to better separate the effects of pressure on octahedral tilting and bond compression, since the tilt plane and Jahn–Teller distortions are orthogonal.

Both Sr_2CuWO_6 and Ba_2CuWO_6 are tetragonally distorted and crystallize in space group $I4/m$ [4–6,12,13]. The large tolerance factor Ba_2CuWO_6 (tol. = 1.04) is typically observed for cubic perovskites, however, the Cu–O–W bond angles in Sr_2CuWO_6 and Ba_2CuWO_6 are nonlinear, indicating that some octahedral tilting is present [6,12]. Application of the intensive variables, e.g. pressure and temperature, are well-known to influence the structures and properties of perovskite-related materials. For example, examination of the crystal structures and magnetic properties of A_2CuWO_6 (A = Ba, Sr) found that the strength of the superexchange interactions correlate well

*Corresponding author. Fax: +1 803 777 8508.
E-mail addresses: zurloye@mail.chem.sc.edu, jssc@mail.chem.sc.edu (H.-C.z Loye).

0022-4596/$ - see front matter © 2006 Elsevier Inc. All rights reserved.
doi:10.1016/j.jssc.2006.07.016

with the octahedral tilting and the resulting Cu–O–W bond angles [6]. Upon heating, the Cu–O–W bond angle of Sr_2CuWO_6 increases and a sequence of phase transitions from $I4/m$ to $I4/mmm$ to $Fm\bar{3}m$ is observed [12]. Pressure has also been shown to induce a phase transition and change in the octahedral tilting in the ordered double perovskites Ba_2BiTaO_6, [14] Ba_2YTaO_6, [15] and Ba_2BiSbO_6 [16]. At low pressures, the dominant compression mechanism is often bond shortening, whereas at high pressures octahedral tilting becomes increasingly important [15,17]. The ordered double perovskites Sr_2CuWO_6 and Ba_2CuWO_6 have octahedral tilting in their ambient pressure structure and also contain long Cu–O bonds as a result of the cooperative Jahn–Teller distortion. It is these characteristics that make Sr_2CuWO_6 and Ba_2CuWO_6 model systems in which to investigate the influence of pressure on the crystal structure in comparison to the ordered double perovskites Sr_2CoMoO_6 and La_2LiRuO_6, which contain symmetric octahedra. In this contribution, we report the bulk modulus of the phases through the use of high-pressure synchrotron studies and contrast the compression mechanisms present in the ordered double perovskites.

2. Experimental

Polycrystalline Ba_2CuWO_6, Sr_2CuWO_6, La_2LiRuO_6 and Sr_2CoMoO_6 were prepared by conventional solid state techniques using appropriate stoichiometric mixtures of high purity $SrCO_3$, $BaCO_3$, La_2O_3, Li_2CO_3, RuO_2, CuO, $CoMoO_4$, and WO_3 and heating for several days with intermediate regrinding until the diffraction pattern no longer changed. Phase purity was established by powder X-ray diffraction using a Rigaku D/MAX 2200 diffractometer. Sr_2CuWO_6 or Ba_2CuWO_6 was the dominant phase with ~2% $SrWO_4$ or $BaWO_4$. The presence of between 2% and 10% by weight of $SrWO_4$ has also been previously reported in the synthesis of Sr_2CuWO_6 [12,13]. In situ high pressure synchrotron X-ray powder diffraction experiments were performed using a diamond anvil cell (DAC) at the X7A beam-line at the National Synchrotron Light Source (NSLS) at Brookhaven National Laboratory (BNL). The primary white beam from the bending magnet was monochromatized and focused using an asymmetrically cut bent Si (111) crystal. A tungsten wire crosshair was positioned at the center of the goniometer circle and subsequently the position of the incident beam was adjusted to the crosshair. A gas proportional position-sensitive detector (PSD) was stepped in 0.25° intervals over the angular range of 5–35° in 2θ with counting times of 60–75 s per step. The wavelength of the incident beam, 0.64824(4) Å for Ba_2CuWO_6, Sr_2CuWO_6, and Sr_2CoMoO_6, and 0.68405(4) Å for La_2LiRuO_6, and PSD zero channel and PSD degrees/channel were determined from a CeO_2 standard (SRM 674). Polycrystalline samples were loaded into the DAC at ambient pressure and room temperature along with a few small ruby spheres. The DAC is based on a modified Merrill–Bassett design and employs two diamonds with 0.5 mm diameter culets on tungsten-carbide supports. The X-rays are admitted by a 0.5 mm diameter circular aperture, and the exit beam leaves via a $0.5 \times 3.0\,mm^2$ rectangular tapered slit, oriented perpendicular to the horizontal plane of the diffractometer. The sample chamber is composed of a ~100 μm diameter hole made using a spark-erosion method in the center of a 250 μm thick stainless-steel gasket, preindented to 150 μm thickness before erosion. The DAC was placed on the second axis of the diffractometer, and the sample position was adjusted using a precentered microscope. The pressure at the sample was measured by detecting the shift in the R1 emission line of the included ruby. No evidence of nonhydrostatic conditions or pressure anisotropy were detected during our experiments, and the R1 peaks from three included ruby chips remained strong and sharp with deviations in the measured pressure of less than 0.15 GPa. A methanol–ethanol–water mixture with component ratio of 16:3:1 was used as a pressure medium. Diffraction data analysis was performed using GSAS with the EXPGUI interface [18]. Uncertainties in the wavelengths were propagated to the lattice parameters obtained from the refinements. A pseudo-Voigt function was used to model the peaks. The angular range employed in the refinements was from 6° to 35° 2θ and excluded the regions which contained strong Bragg peaks from the pressure cell gasket and $BaWO_4$ phase.

3. Results and discussion

Examination of the systematic extinctions of the laboratory X-ray powder diffraction measurements resulted in a tetragonal body-centered unit cell for Ba_2CuWO_6, Sr_2CuWO_6 and Sr_2CoMoO_6. The structures were described with space group $I4/m$ and starting atomic positions taken from previous crystal structure analyses [6,12,19]. La_2LiRuO_6 has a monoclinic unit cell and space group $P2_1/n$ [20]. Refinement of the complete crystal structures of La_2LiRuO_6, Sr_2CoMoO_6, and Sr_2CuWO_6 was not possible at elevated pressures, in part because of the gasket contribution and structural complexity of each, the peak overlap present in La_2LiRuO_6, and pseudosymmetry and peak overlap in Sr_2CoMoO_6. A LeBail analysis was used to extract the lattice parameters and unit cell volume of Sr_2CuWO_6 and Sr_2CoMoO_6. The monoclinic symmetry of La_2LiRuO_6 resulted in substantial peak overlap, poor fits, and unphysical changes in the lattice parameters with pressure during the LeBail refinements. In order to overcome this difficulty, a constrained Rietveld refinement was undertaken with the hypothetical crystal structure fixed using the software program SPuDS, which has previously been shown to generate accurate structures of perovskite compounds [21]. This approach has the advantage that the relative intensities of the peaks are constrained in the refinement, which results in more stable refinements and reasonable lattice parameters and unit cell

volumes. Although no changes in the structure of La_2LiRuO_6 with pressure were considered, the changes in tilting and the structure are generally relatively small in the absence of a structural phase transition. The large $c/\sqrt{2}a$ ratio of Ba_2CuWO_6 and the substantial splitting of the main reflections enabled refinement of the crystal structures of Ba_2CuWO_6 using data collected at pressures up to approximately 2.5 GPa. The atomic displacement parameters were held constant during the Rietveld refinements with the $U_{iso} = 0.015\,Å^2$. Attempts to refine the crystal structure of Ba_2CuWO_6 above 2.5 GPa resulted in large uncertainties in the oxygen positions and unreasonable bond distances, therefore LeBail refinements were used to obtain the lattice parameters at pressures above 2.5 GPa. There was no indication of any pressure-induced phase transition in the investigated pressure range in each of the compounds examined in this study.

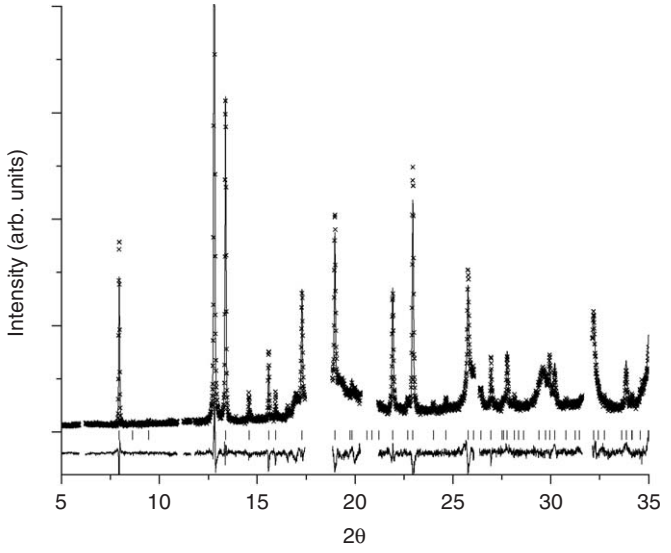

Fig. 1. Rietveld refinement of Ba_2CuWO_6 with data collected at 0.6(2) GPa. Observed (circle), calculated (line), and difference (bottom) profiles are given using a structure model with space group $I4/m$. Regions containing significant contribution from the gasket and $BaWO_4$ were excluded.

A plot of the Rietveld refinement of Ba_2CuWO_6 at an applied pressure of 0.6(2) GPa is shown in Fig. 1. The crystal structures of Ba_2CuWO_6 and Sr_2CoMoO_6 are shown in Fig. 2. In Ba_2CuWO_6 and Sr_2CuWO_6, the long Cu–O bonds (~2.4 Å) are aligned along the c-axis, whereas Cu–O bonds in the ab plane are significantly shorter (~2.0 Å). In contrast, the octahedra in Sr_2CoMoO_6 and La_2LiRuO_6 have a relatively small difference between the longest and shortest bond in each [BO_6] octahedra. The pressure dependence of the lattice parameters and unit cell volumes of Sr_2CuWO_6, Ba_2CuWO_6, Sr_2CoMoO_6, and La_2LiRuO_6 are given in Tables 1–4, respectively. The approximate bulk moduli were determined by fitting the pressure dependence of the unit cell volume to a second-order Birch–Murnaghan equation of state and are 153(6) GPa for Ba_2CuWO_6, 185(14) for Sr_2CuWO_6, 152(9) GPa for Sr_2CoMoO_6, and 106(8) GPa for La_2LiRuO_6. The narrow pressure range limits the accuracy of the fitting procedure to determine the bulk moduli and, therefore, should be viewed with caution. The bulk moduli are typical and are comparable to other ordered double perovskites, for example, Ba_2BiTaO_6 at 126(10) GPa, [14] $Ba_2PrRu_{0.8}Ir_{0.2}O_6$ at 139(10) GPa, [22] Ba_2YTaO_6 at 157(16) GPa, [23] $Sr_2TbRu_{0.3}Ir_{0.7}O_6$ at 196(10) GPa [24]. The small bulk modulus of La_2LiRuO_6 is similar to $SrCeO_3$ with a bulk modulus of 110.1(6) GPa, [25] where the atypical compressibility behavior of $SrCeO_3$ was attributed to the magnitude of the long ($\approx$2.23 Å) Ce–O bonds [25]. Similarly, in the case of La_2LiRuO_6 the relatively small bulk modulus might be attributed to the high compressibility of the long Li–O bonds ($\approx$2.08 Å).

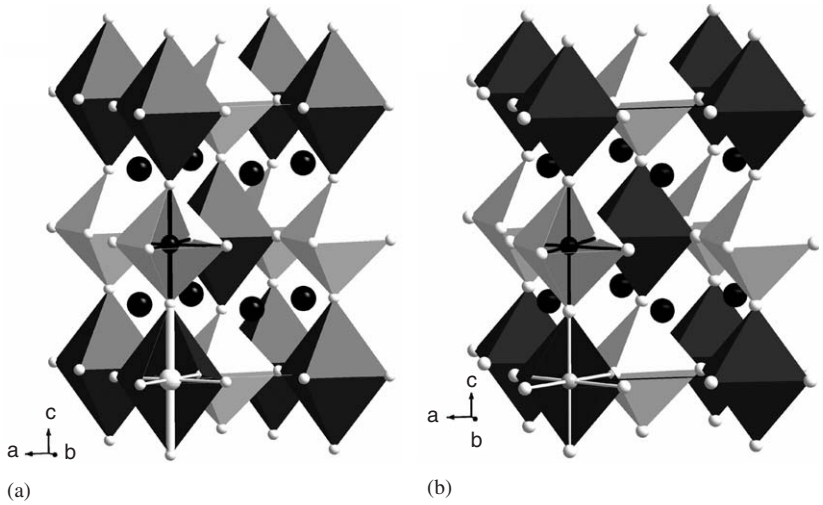

Fig. 2. (a) Crystal structure of Ba_2CuWO_6. Large black spheres are Ba, small spheres are O, and Cu and W are located at the center of the dark and light octahedra, respectively. The long Cu–O bonds are oriented parallel to the c-axis and are thicker. (b) Crystal structure of Sr_2CoMoO_6. Large black spheres are Sr, small spheres are O, and Mo and Co are located at the center of the dark and light octahedra, respectively.

Table 1
Pressure dependence of the lattice parameters and unit cell volume of Sr_2CuWO_6

Pressure (GPa)	a (Å)	c (Å)	Vol. (Å^3)
0.4	5.4300(3)	8.4138(7)	248.08(3)
0.8	5.4252(5)	8.3997(11)	247.22(4)
2.4	5.4097(5)	8.3652(12)	244.81(5)
2.8	5.4072(3)	8.3605(5)	244.44(2)
3.4	5.4024(4)	8.3484(11)	243.66(4)
4.1	5.3952(4)	8.3346(10)	242.61(4)
4.8	5.392(1)	8.330(2)	242.23(9)
5.8	5.389(1)	8.321(2)	241.63(9)

Table 2
Pressure dependence of the lattice parameters and unit cell volume of Ba_2CuWO_6

Pressure (GPa)	a (Å)	c (Å)	Vol. (Å^3)
0.6	5.5640(2)	8.6269(5)	267.07(2)
0.9	5.5635(2)	8.6184(4)	266.76(1)
1.4	5.5586(2)	8.5989(4)	265.69(1)
2.0	5.5554(3)	8.5750(4)	264.65(2)
2.5	5.5523(2)	8.5584(4)	263.84(1)
3.0	5.5475(2)	8.5413(4)	262.54(2)
4.0	5.5420(3)	8.5155(5)	261.20(2)

Table 3
Pressure dependence of the lattice parameters and unit cell volume of Sr_2CoMoO_6

Pressure (GPa)	a (Å)	c (Å)	Vol. (Å^3)
0.2	5.5734(3)	7.9625(4)	247.34(2)
0.8	5.5602(2)	7.9490(3)	245.749(6)
1.6	5.5472(2)	7.9373(3)	244.239(6)
3.0	5.5285(2)	7.9185(3)	242.026(8)
5.1	5.5057(2)	7.8980(3)	239.412(7)
6.3	5.4946(2)	7.8919(3)	238.264(8)

Table 4
Pressure dependence of the lattice parameters and unit cell volume of La_2LiRuO_6

Pressure (GPa)	a (Å)	b (Å)	c (Å)	β (deg)	Vol. (Å^3)
0.5	5.5527(4)	5.6114(3)	7.8399(5)	89.99(4)	244.28(2)
1.2	5.548(1)	5.609(1)	7.821(2)	89.9(1)	243.42(4)
2.2	5.533(3)	5.603(3)	7.794(4)	90.0(2)	241.63(9)
3.4	5.532(3)	5.574(3)	7.745(4)	88.76(3)	238.80(6)
4.6	5.514(2)	5.556(3)	7.712(3)	88.08(3)	236.15(6)

It is noteworthy that the bulk modulus of Ba_2CuWO_6 is smaller than that of Sr_2CuWO_6. Fig. 3 shows the pressure dependence of the lattice parameters and illustrates the decrease in the a and c lattice parameters. A least squares fit was performed to extract the linear pressure dependence of the lattice parameters using $a(P) = a_0(1 - \kappa_a P)$, where a_0 is the zero pressure lattice parameter κ_a is the linear

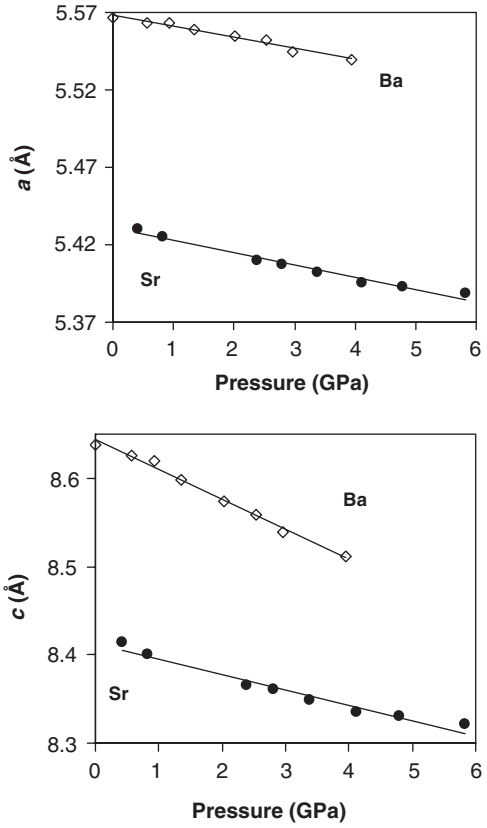

Fig. 3. Pressure dependence of the lattice parameters of Ba_2CuWO_6 (diamonds) and Sr_2CuWO_6 (filled circles) in space group $I4/m$. Lines indicate least squares fits to the data.

compressibility, and P is the pressure. Table 5 contains the axial compressibility for each compound in this study. The axial compressibility of the a and b lattice parameters of La_2LiRuO_6 are smaller than that found for the c lattice parameter. It is noteworthy that for La_2LiRuO_6 in-phase tilting occurs parallel to the c-axis, whereas the out of phase octahedral tilting occurs in the ab plane. However, the beta angle tends to decrease with increasing pressure, which is consistent with increased octahedral tilting. We are hesitant to attribute any compression mechanism to this feature, since in the monoclinic space group there is substantial peak overlap that obscures the relationship between summed peak intensities and the individual lattice parameters; consequently, correlations between the beta angle and a and c are reduced in the unit cell volume. Unfortunately, the data do not allow for complete structure refinements that are necessary to further investigate the detailed structural changes responsible for the differences in axial compressibility.

Two notable differences are evident in the axial compressibility of the compounds in this study. Firstly, a large difference is observed in the axial compressibility of the c-axis of Ba_2CuWO_6 compared to Sr_2CuWO_6, whereas a smaller difference is found between the compressibility of the a-axes. Secondly, the axial compressibility of a is smaller than c for Ba_2CuWO_6 and Sr_2CuWO_6, whereas the

opposite occurs for Sr_2CoMoO_6, where the axial compressibility of a is larger than that of c. As further illustration, the lattice parameter ratio, $c/(\sqrt{2}a)$, is shown in Fig. 4 for isostructural Ba_2CuWO_6, Sr_2CuWO_6, and Sr_2CoMoO_6. It is immediately evident that the $c/(\sqrt{2}a)$ ratio decreases for Ba_2CuWO_6 and Sr_2CuWO_6, whereas the $c/(\sqrt{2}a)$ ratio increases for Sr_2CoMoO_6. It is also evident that the $c/(\sqrt{2}a)$ ratio decreases more rapidly for Ba_2CuWO_6 than for Sr_2CuWO_6.

In order to further investigate the changes in the Cu–O bonds, the results of the Rietveld refinements on the structure of Ba_2CuWO_6 are shown in Table 6, which lists the pressure dependence of the structural parameters and selected bond lengths and angles. In unconstrained refinements, the scatter in the Cu–O(2)–W bond angles indicated that the real uncertainty was larger than the uncertainty calculated from the refined structure. We therefore constrained the position of O(2) and refined the position of O(1). The pressure dependence of the Cu–O bond lengths of Ba_2CuWO_6 are graphically shown in Fig. 5. Although the relatively large uncertainty in the oxygen position results in a relatively large uncertainty in the metal oxygen bond distances, there is an apparently preferential compression of the Cu–O(1) bond with an increase in the applied pressure, which is also responsible for the rapid decrease in the c lattice parameter. This feature may be rationalized by considering that the long Cu–O(1) bond is more compressible than the short W–O(1) bond due to the high valence of W^{6+}. The less rapid decrease in the $c/(\sqrt{2}a)$ ratio of Sr_2CuWO_6 suggests that the Cu–O(1) bond of Sr_2CuWO_6 is slightly less compressible than the one in Ba_2CuWO_6. At ambient pressure, the $c/(\sqrt{2}a)$ values are very similar at 1.0975 and 1.0962 for Ba_2CuWO_6 and Sr_2CuWO_6, respectively. The relationship of the compressibility of the $[SrO_{12}]$ and $[BaO_{12}]$ dodecahedra and the octahedral tilting are suggested to play a role in the compressibility differences. A recent investigation of the high-pressure behavior of tetragonal ordered double perovskites indicates that the increase in the $c/(\sqrt{2}a)$ ratio is evidence for an increase in the magnitude of anti-phase octahedral tilting [26]. An increase in the magnitude of the octahedral tilting distortion may be one reason for the less rapid decrease in the lattice parameter ratio of Sr_2CuWO_6, since an increase in the magnitude of the octahedral tilting distortion would increase the $c/(\sqrt{2}a)$ ratio, counteracting Cu–O(1) bond shortening. The decrease in the lattice parameter ratio for both Ba_2CuWO_6 and Sr_2CuWO_6 suggests the compression of the long Cu–O(1) bond is still the dominant compression mechanism, although the contribution of octahedral tilting is a more significant factor for Sr_2CuWO_6 than for Ba_2CuWO_6. Anisotropic compression of Cu–O bonds has also been previously observed in high-pressure studies of other cuprates

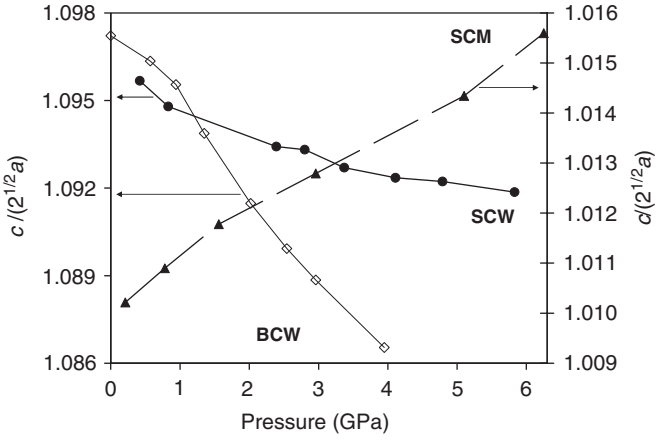

Fig. 4. Pressure dependence of the lattice parameter ratio $c/(\sqrt{2}a)$of Ba_2CuWO_6 [BCW] (diamonds), Sr_2CuWO_6 [SCW] (filled circles), and Sr_2CoMoO_6 [SCM] (filled triangles) in space group $I4/m$. Lines are guides to the eye.

Table 5
Axial compressibility of Ba_2CuWO_6, Sr_2CuWO_6, Sr_2CoMoO_6 and La_2LiRuO_6

κ ($\times 10^{-3}$)	Ba_2CuWO_6	Sr_2CuWO_6	Sr_2CoMoO_6	La_2LiRuO_6
$\kappa(a)$	1.21(5)	1.5(1)	2.3(1)	1.6(2)
$\kappa(b)$	—	—	—	2.5(4)
$\kappa(c)$	3.9(2)	2.1(2)	1.4(1)	4.1(2)

Table 6
Pressure dependence of the structural parameters and selected bond lengths and angles for Ba_2CuWO_6

Pressure (GPa)	0.6	0.9	1.4	2.0	2.5
O(1) z	0.271(3)	0.269(3)	0.270(3)	0.270(4)	0.268(3)
Cu–O(1) (Å) ($\times 2$)	2.34(3)	2.32(3)	2.33(3)	2.31(4)	2.30(2)
Cu–O(2) (Å) ($\times 4$)	2.05	2.05	2.05	2.05	2.05
W–O(1) (Å) ($\times 2$)	1.98(3)	1.99(3)	1.97(3)	1.98(4)	1.98(2)
W–O(2) (Å) ($\times 4$)	1.95	1.95	1.95	1.95	1.95
R_{wp} (%)	10.46	7.87	8.05	9.51	7.65
R_p (%)	8.08	5.85	6.22	7.55	5.45
χ^2	4.58	4.50	5.44	5.61	5.65

Atoms on fixed positions are Ba (0, 1/2, 1/4), Cu (0, 0, 0), W(0, 0, 1/2), O(1) (0, 0, z), O(2) (x, y, 0). The O(2) fractional coordinates were fixed at (0.2098, 0.3035, 0).

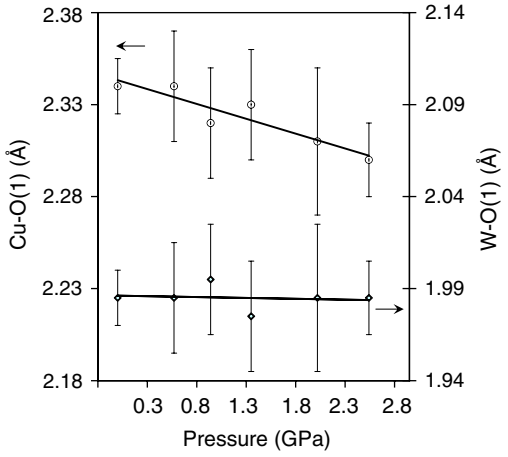

Fig. 5. Pressure dependence of Cu–O(1) and W–O(1) bond lengths in Ba_2CuWO_6. Linear trendlines are shown to guide the eye.

[27,28,28–31]. In contrast, octahedral tilting appears to be the governing compression mechanism in the case of Sr_2CoMoO_6.

In summary, we have examined four ordered double perovskites by high-pressure synchrotron powder diffraction. Bulk moduli were determined by fitting the volume–pressure data using a second-order Birch–Murnaghan equation of state. The pressure dependence of the lattice parameters of Ba_2CuWO_6 was significantly more anisotropic than Sr_2CuWO_6. In each compound of this study, both bond compression and octahedral tilting play a prominent role, with bond compression prevailing over octahedral tilting, most notably, in the strongly distorted Ba_2CuWO_6.

Acknowledgments

Financial support from the Department of Energy through Grant DE-FG02-04ER46122 and the National Science Foundation through Grant no. DMR:0450103 is gratefully acknowledged. Work at Brookhaven is supported by the US Department of Energy, Division of Materials Sciences, under contract no. DE-AC02-98CH10886.

References

[1] R.H. Mitchell, Perovskites: Modern and Ancient, Almaz Press, Ont., Canada, 2002.
[2] M.T. Anderson, K.B. Greenwood, G.A. Taylor, K.R. Poeppelmeier, Prog. Solid State Chem. 22 (1993) 197.
[3] Y.N. Venevtsev, Mater. Res. Bull. 6 (1971) 1085.
[4] D. Reinen, H. Weitzel, Z. Anorg. Allg. Chem. 424 (1976) 31.
[5] Bokhimi, Powder Diffr. 7 (1992) 228.
[6] D. Iwanaga, Y. Inaguma, M. Itoh, J. Solid State Chem. 147 (1999) 291.
[7] Y. Todate, J. Phys. Soc. Japan 70 (2001) 337.
[8] D. Reinen, H.O. Wellern, J. Wegwerth, Z. Phys. B Condens. Matter 104 (1997) 595.
[9] H. Jahn, E. Teller, Proc. R. Soc. Ser. A 161 (1937) 220.
[10] J. Kanamori, J. Appl. Phys. 31 (1960) 14S.
[11] M.W. Lufaso, P.M. Woodward, Acta Crystallogr. B 60 (2004) 10.
[12] M. Gateshki, J.M. Igartua, J. Phys.: Condens. Matter 15 (2003) 6749.
[13] M. Gateshki, J.M. Igartua, E. Hernandez-Bocanegra, J. Phys.: Condens. Matter 15 (2003) 6199.
[14] K.S. Wallwork, B.J. Kennedy, Q.D. Zhou, Y. Lee, T. Vogt, J. Solid State Chem. 178 (2005) 207.
[15] M.W. Lufaso, R.B. Macquart, Y. Lee, T. Vogt, H.-C. zur Loye, Chem. Commun. (2006) 168.
[16] M.W. Lufaso, R. Macquart, Y. Lee, T. Vogt, H.-C. zur Loye, J. Solid State Chem. 179 (2006) 917.
[17] H.Z. Liu, J. Chen, J. Hu, C.D. Martin, D.J. Weidner, D. Hausermann, H.K. Mao, Geophys. Res. Lett. 32 (2005).
[18] A.C. Larson, R.B. von Dreele, General Structure Analysis System (GSAS), Los Alamos National Laboratories, 1990.
[19] M.C. Viola, M.J. Martinez-Lope, J.A. Alonso, P. Velasco, J.L. Martinez, J.C. Pedregosa, R.E. Carbonio, M.T. Fernandez-Diaz, Chem. Mater. 14 (2002) 812.
[20] P.D. Battle, C.P. Grey, M. Hervieu, C. Martin, C.A. Moore, Y. Paik, J. Solid State Chem. 175 (2003) 20.
[21] M.W. Lufaso, P.M. Woodward, Acta Crystallogr. B 57 (2001) 725.
[22] B.J. Kennedy, L.Q. Li, Y. Lee, T. Vogt, J. Phys.: Condens. Matter 16 (2004) 3295.
[23] M.W. Lufaso, R.B. Macquart, Y. Lee, T. Vogt, H.-C. zur Loye, Chem. Commun. (2006) 168.
[24] Q. Zhou, B.J. Kennedy, K.S. Wallwork, M.M. Elcombe, Y. Lee, T. Vogt, J. Solid State Chem. 178 (2005) 2282.
[25] K.S. Knight, W.G. Marshall, N. Bonanos, D.J. Francis, J. Alloys Compds. 394 (2005) 131.
[26] M.W. Lufaso, R.B. Macquart, Y. Lee, T. Vogt, H.-C. zur Loye, J. Phys.: Condens. Matter (2006), submitted for publication.
[27] A.L. Cornelius, J.S. Schilling, Physica C 218 (1993) 369.
[28] A.R. Armstrong, W.I.F. David, I. Gameson, P.P. Edwards, J.J. Capponi, P. Bordet, M. Marezio, Phys. Rev. B 52 (1995) 15551.
[29] H. Wilhelm, C. Cros, E. Reny, G. Demazeau, M. Hanfland, J. Mater. Chem. 8 (1998) 2729.
[30] H. Ehrenberg, J.A. McAllister, W.G. Marshall, J.P. Attfield, J. Phys.: Condens. Matter 11 (1999) 6501.
[31] N.C. Hyatt, J.A. Hriljac, Y. Miyazaki, I. Gameson, P.P. Edwards, Phys. Rev. B 65 (2002).